Quantum-mechanical analysis of the equation of state of anatase TiO_2

M. Calatayud,[1] P. Mori-Sánchez,[2] A. Beltrán,[1] A. Martín Pendás,[2] E. Francisco,[2] J. Andrés,[1] and J. M. Recio[1,2]
[1]*Departament de Ciències Experimentals, Universitat Jaume I, E-12080 Castelló, Spain*
[2]*Departamento de Química Física y Analítica, Universidad de Oviedo, E-33006 Oviedo, Spain*
(Received 30 May 2001; published 23 October 2001)

Quantum-mechanical simulations have been performed to investigate pressure effects on the crystal geometry, chemical bonding, and the electronic structure of anatase TiO_2. Total energy calculations are carried out using the density functional formalism under the nonlocal B3LYP approximation. The optimized unit cell equilibrium parameters and the bulk and linear compressibilities are determined to be in good agreement with recent experimental data. The topology of the electron density is examined by means of the atoms in molecules (AIM) theory. Computed AIM charges and topological properties of the bond critical points reveal a partially ionic behavior of the crystal that complements the description obtained from the band structure and the projected density of states analysis. A microscopic interpretation of the crystal response to hydrostatic pressure is given in terms of the elementary polyhedra and the AIM atomic volumes that fill the unit cell space.

DOI: 10.1103/PhysRevB.64.184113 PACS number(s): 64.30.+t, 61.50.Ah, 71.15.Nc, 71.20.−b

I. INTRODUCTION

The anatase phase of titanium dioxide raises a great interest in a wide range of scientific and industrial fields such as the photochemistry of solar cells, ceramics, catalysis, pigments, and optoelectronics.[1–4] Many of these applications rely on the good performance of this material under variable conditions of temperature and hydrostatic pressure, exposure to electromagnetic radiation, and surface reactivity with a variety of chemical agents. The investigation of the fundamental properties of this polymorph appears to be crucial in order to understand such interesting behavior. Although comparatively to the rutile structure anatase was claimed to have received less attention, new experimental and theoretical results are now stimulating the study of the structural, elastic, electronic, and optical properties of this polymorph.[5–8]

Recently, high-pressure measurements have characterized the rich polymorphism of TiO_2 using single-crystal and polycrystalline anatase as the starting material.[6] The volume-pressure room-temperature data yield values for anatase bulk modulus ($B_0=179\pm2$ GPa in single crystals and 190 ± 10 GPa in polycrystalline samples) in sharp contrast with the other two known experimental data ($B_0=59\pm5$ GPa, Ref. 9, and $B_0=360$ GPa, Ref. 10). Previous theoretical values of B_0 ranged from 194 GPa (Ref. 11) to 272 GPa (Ref. 12). The most recent quantum-mechanical calculations[6,7] and atomistic simulations[8] predict B_0 to be around 190 GPa, giving thus support to the experimental equation of state (EOS) of Arlt *et al.* The scattering in the reported data demands a comprehensive interpretation of the response of the crystalline structure to hydrostatic pressure beyond the evaluation of EOS parameters. A detailed decomposition of the crystal compressibility in terms of linear (lattice parameters and bond lengths) and volumetric (polyhedral and atomic) contributions becomes appropriate to evaluate the proposed EOS. Such an analysis has proved to be useful to explain the pressure behavior of alkali halides and several nitrogen- and oxygen-based spinels.[13–15] Given its predictive capabilities, it is worthwhile to extend this type of analysis to the anatase structure.

The electronic structure of anatase is also a subject of debate, as shown by the discrepancies among the theoretical studies reported so far. First-principles pseudopotential[7] (PS), all-electron[5] (AE), and orthogonalized linear combination of atomic orbitals[12] (OLCAO) calculations within the local density approximation (LDA) are qualitatively consistent with each other, but disagreement with the PS Hartree-Fock results of Fahmi *et al.*[16] has been pointed out[5] ''even in the valence bands.'' Moreover, the band gap is predicted to be indirect according to the PS- and OLCAO-LDA analyses, but direct when computed at the AE-LDA optimized equilibrium geometry. Asahi *et al.*[5] concluded that the nature of the band gap is ''quite sensitive to the crystal configuration'' since they obtained the same kind of indirect absorption edge as Mo and Ching[12] ($M\rightarrow\Gamma$) when the experimental lattice parameters were chosen. Mikami *et al.*[7] found the minimum band gap between the conduction band at Γ and the valence band near X (and not M) because the high-symmetry directions of the Brillouin zone (BZ) should correspond to a body-centered tetragonal lattice, and not to a simple tetragonal one as in rutile. All these calculations estimated the band gap around 1.4 eV below the experimental value of 3.2 eV,[17] due to the inherent shortcomings associated with the LDA. Analyses of the electronic density of states (DOS) have been presented by Fahmi *et al.*,[16] Mo and Ching,[12] and Ashami *et al.*[5] Core and valence DOS have also been investigated from the photoemission spectromicroscopy experiments of Sanjinés *et al.*[18] and implications related to chemical bonding in anatase deduced.

It is then desirable to use the correct BZ geometry together with nonlocal exchange-correlation functionals in order to obtain reasonable anatase band structures at changing unit cell geometries. The outcome of this exploration should contribute to clarify some of the questions posed in previous works. It is also interesting to complement these results with the less common analysis of the topology of the electron density in the light of the atoms in molecules (AIM) formalism.[19] Within the AIM framework, a quantum system is rigorously partitioned into subsystems that obey the general quantum-mechanical rules. In this way it is possible, for

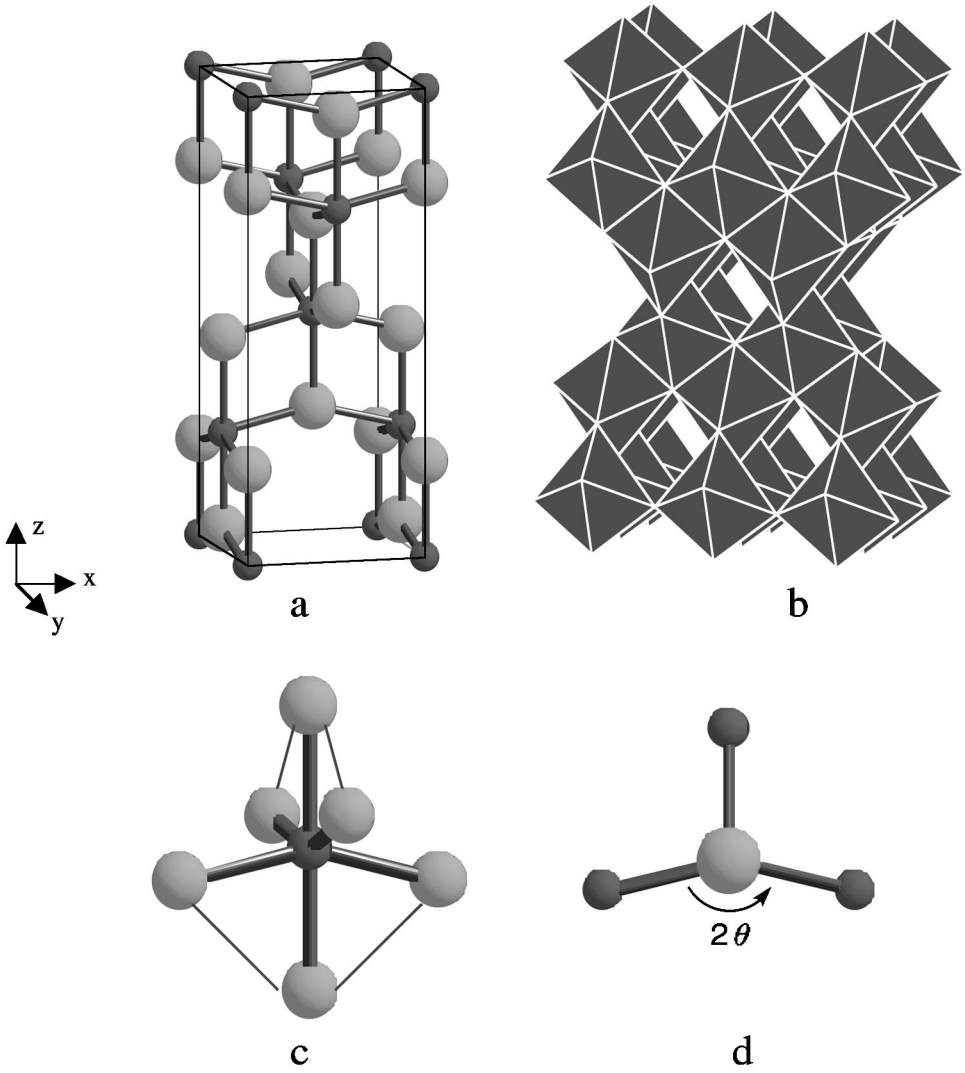

FIG. 1. Crystal structure of anatase TiO_2. (a) Unit cell. (b) Cation polyhedra. (c) Local environment of Ti. (d) Local environment of O.

instance, to obtain definite sizes and charges for the atomic components of the crystal, identify the bonding network of the crystal, and characterize the nature of the chemical bonds in terms of the properties of the charge density and its Laplacian.[20]

In the present investigation, we perform first-principles density functional computations using the standard nonlocal exchange-correlation functionals provided by the CRYSTAL (Ref. 21) package. The two main objectives of this work can be outlined as follows. First, we try to provide new accurate theoretical results concerning the EOS parameters, the band structure description, and the characteristics of the chemical bonding in the anatase phase of TiO_2. Second, we pursue to perform a critical analysis of the bulk compressibility by investigating the pressure-induced effects on the unit cell elementary polyhedra and the atomic constituents of the crystal. The rest of the paper is divided into three sections. In the next one, modeling and methodological aspects are introduced. Section III contains the main results together with the discussion concerning the equilibrium cell geometry, band structure, Bader chemical graph, and pressure effects on these magnitudes. Finally, we summarize our main conclusions in Sec. IV.

II. METHODOLOGICAL DETAILS AND COMPUTATIONAL STRATEGY

A. Structural description

The anatase structure of TiO_2 is one of the prototypes of 6:3 lattices, and belongs to the $I4_1/amd$ space group. The conventional unit cell [Fig. 1(a)] contains four TiO_2 units, and there is only one internal parameter related to the oxygen location. Titanium atoms occupy the $4a$ Wyckoff position at $(0,0,0)$, and all oxygens are equivalent and located at the $8e$ $(0,0,u)$ position. The local symmetries of both nuclei are D_{2d} and C_{2v}, respectively. The structure is usually described as composed of chains of vertex-linked distorted TiO_6 octahedra that share alternating edges [see Fig. 1(b)]. There are two different Ti-O distances in these octahedra: (i) a long one involving the two oxygen atoms directed along the c crystallographic axis (apical oxygens), which we label $d^{\mathrm{ap}}_{\mathrm{Ti\text{-}O}}$; (ii) a short one, $d^{\mathrm{eq}}_{\mathrm{Ti\text{-}O}}$, with the four equatorial oxygens left, which are arranged forming a tetrahedron squeezed along one of its C_2 axes. The degree of squeezing is measured by the u parameter, the limiting planar situation corresponding to $u=1/4$. There are three different O-O distances in the octahe-

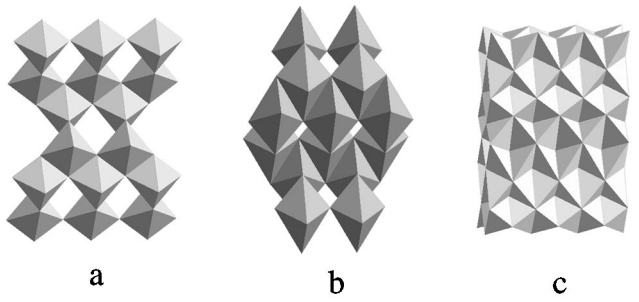

FIG. 2. Volume decomposition in polyhedral arrays. (a) TiO_6 occupied octahedra. (b) O_6 empty octahedra. (c) O_4 empty tetrahedra.

dron: $d^{eq}_{O\text{-}O}$ between equatorial oxygens, $d^{sh}_{O\text{-}O}$ between an apical oxygen and an equatorial oxygen belonging to a shared edge, and $d^{ush}_{O\text{-}O}$ between an apical oxygen and an equatorial oxygen of an unshared edge of the octahedron [see Fig. 1(c)]. Oxygens are located along the C_2 axis of isosceles triangles of Ti atoms, and their distances to them are $d^{eq}_{Ti\text{-}O}$ (two) and $d^{ap}_{Ti\text{-}O}$ (one); the Ti-O-Ti angle between the two shortest bonds is called 2θ [see Fig. 1(d)]. The algebraic expressions of these parameters as functions of the lattice parameters a, c, and u are as follows:

$$d^{ap}_{Ti\text{-}O}=cu, \quad d^{eq}_{Ti\text{-}O}=\sqrt{\frac{1}{4}a^2+c^2\left(u-\frac{1}{4}\right)^2},$$

$$d^{eq}_{O\text{-}O}=\sqrt{\frac{1}{2}a^2+c^2\left(2u-\frac{1}{2}\right)^2}, \tag{1}$$

$$d^{sh}_{O\text{-}O}=\sqrt{\frac{1}{4}a^2+c^2\left(2u-\frac{1}{4}\right)^2},$$

$$d^{ush}_{O\text{-}O}=\sqrt{\frac{1}{4}a^2+\frac{1}{16}c^2}, \quad 2\theta=2\arcsin\frac{a}{2d^{eq}_{Ti\text{-}O}}. \tag{2}$$

There are four occupied TiO_6 octahedra per unit cell. The rest of the space in the unit cell may be described with the help of anionic polyhedra lacking inner cations. These are called empty polyhedra. In the anatase structure there are 4 empty O_6 octahedra and 16 empty O_4 tetrahedra, as shown in Fig. 2. The geometrical centers of the former occupy the $4b$ Wyckoff positions at $(0,0,\frac{1}{2})$. These sites are crystallographically equivalent to the $4a$ cationic locations, and therefore have D_{2d} symmetry. The empty tetrahedra are much less symmetric. Their geometrical centers are located at the $16f$ $(\frac{1}{4},\frac{1}{4},\frac{3}{8})$ point and display just a C_2 axis parallel parallel to the a or b crystallographic directions. The empty O_6 octahedra form chains that are analogous to those of the occupied ones. The four unshared edges involving the apical oxygen belong simultaneously to both types of octahedra, but no faces are shared. The free space between occupied and empty octahedra generates the vertex-linked tetrahedra array.

B. Total energy

Calculations were performed with the CRYSTAL98 program package,[21] using a 6-31G basis set developed by Rassolov *et al.*[22] for both titanium and oxygen atoms. The convergence in the total energy ($E_{crystal}$) was assured to be better than 10^{-5}. Becke's three-parameter hybrid nonlocal exchange functional[23] combined with the Lee-Yang-Parr gradient-corrected correlation functional,[24] B3LYP, has been used. Hybrid density functional methods have been extensively used for molecules and provide also an accurate description of crystalline structures as bond lengths, binding energies, and bang gap values are regarded.[25] The band structure was obtained at 59 $\vec{k}$ points along the appropriate high-symmetry paths of the BZ for a tetragonal body-centered system.[26]

In order to take into account the effect of pressure (p) on this system, we have optimized all the geometrical parameters, a,c,u, at a number of fixed volumes (V) in the range $0.88 \leqslant V/V_0 \leqslant 1.12$, where V_0 is the equilibrium unit cell volume. Different optimization algorithms have been tested to yield similar results, and the less computationally demanding Nelder-Mead method[27] has been finally used. Optimizations have been carried out until the convergence in the energy achieved 10^{-5} a.u.

C. Bader analysis

The AIM theory leads to a partition of the physical space into regions delimited by local zero-flux surfaces (ZFS's) of the electron density gradient $|\vec{\nabla}\rho|$ vector field that are usually associated to the chemist's view of an atom-in-a-molecule. These atomic regions are basins containing all the flux lines ending at a local maximum critical point (CP) of the electron density. These points are usually located at the nuclear positions. Bonded atoms share a portion of their ZFS's called the interatomic surface. This surface contains all the flux lines that finish at a particular $(3,-1)$ saddle CP, called the bond CP (bCP). The only two flux lines that start at the bCP end at the two bonded nuclei, and define the interatomic line of the maximum density or bond path. Bonded atoms are then unequivocally identified by bCP's and their bond path. The rest of the CP's of the crystal are also located on the ZFS's.[20] Rings of bond paths define $(3,+1)$ saddle CP's (ring CP's), and minima of the electron density $[(3,-3)$ CP's] occur inside cages of noncoplanar rings. The physical properties of atomic subsystems are objectively defined in this formalism by integration of the appropriate operator densities within the atomic basins. The properties so defined are additive and build up to yield the global macroscopic properties of the crystal.

We have used the CRITIC (Ref. 29) code to perform a systematic search of CP's within the unit cell that provides the complete topological structure of the crystal's electron density. Atomic properties have also been obtained by numerical integration within the computed atomic basins.

D. EOS fittings and local compressibility decomposition

The EOS of anatase has been obtained by minimizing the enthalpy of the crystal, $H(V)=E_{crystal}(V)+pV$, with respect

to all geometrical parameters at 16 fixed values of p ranging from 0 to 15 GPa. This strategy provides our raw (p,V) data. The zero-pressure bulk modulus (B_0) and its first derivative with respect to p (B_0') are obtained by a fitting procedure using the universal EOS of Vinet *et al.*[30] (VEOS):

$$\frac{px^2}{3(1-x)}=B_0e^{A(1-x)},\quad x=\left(\frac{V}{V_0}\right)^{1/3},\quad A=\frac{3}{2}(B_0'-1). \tag{3}$$

The macroscopic compressibility may be recast in terms of local contributions whenever a complete partition of the unit cell volume into physically significative nonoverlapping subregions is at hand. As we have recently shown, the AIM formalism achieves this goal in a straightforward manner using quantum atoms.[13,15] In this work, we extend this type of analysis considering also the elementary polyhedra generated by the anionic sublattice. The polyhedral volume expanded by TiO_6 octahedra (V_{oct}), empty O_6 octahedra (V_{oct}^o), and empty O_4 tetrahedra (V_{tet}^o) completely fill the space of the anatase unit cell:

$$V=4V_{oct}+4V_{oct}^o+16V_{tet}^o,\quad V_{oct}=\frac{1}{3}a^2cu,$$

$$V_{oct}^o=\frac{1}{3}a^2c\left(\frac{1}{2}-u\right),\quad V_{tet}^o=\frac{1}{48}a^2c. \tag{4}$$

From the topological volumes V_{Ti} and V_O, the relevant expression is simply $V=4V_{Ti}+8V_O$.

All the local compressibilities used in the paper,

$$\kappa_i=\frac{1}{B_i(p)}=-\frac{1}{V_i}\left(\frac{\partial V_i}{\partial p}\right),$$

have been obtained by fitting the VEOS to the appropriate (p,V_i) data. V_i stands for the atomic topological volumes (V_{Ti}, V_O) when considering atomic compressibilities or the polyhedral volumes (V_{oct}, V_{oct}^o, and V_{tet}^o) when polyhedral compressibilities are regarded. Least-squares fittings to the simple quadratic function $V_i(p)=V_i(0)[1-\kappa_i(0)p+\delta_ip^2]$ yield $\kappa_i(0)\equiv\kappa_i$ values differing from those derived from the VEOS by less than 0.1 TPa^{-1} in all cases.

As a consequence of these space-filling partitions, the bulk compressibility of the crystal (κ) can be expressed in terms of the local compressibilities κ_i using the following equation:

$$\kappa=\frac{1}{B_0}=\sum_i f_i\kappa_i,\quad f_i=\frac{n_iV_i}{V}, \tag{5}$$

where i runs over the different regions in which the unit cell is divided and n_i is the number of regions of type i in the cell.

The linear compressibilities

$$\kappa_a=-\frac{1}{a}\left(\frac{\partial a}{\partial p}\right)$$

and

$$\kappa_c=-\frac{1}{c}\left(\frac{\partial c}{\partial p}\right),$$

as well as the fractional change of the internal parameter u with p,

$$\kappa_u=-\frac{1}{u}\left(\frac{\partial u}{\partial p}\right),$$

are also interesting and have been obtained by a least-squares fit to the function $\eta(p)=\eta(0)(1-\kappa_\eta p+\delta p^2)$ $(\eta=a,c,u)$.

It is also relevant to point out that the final values of the compressibilities can be checked for consistency by comparing the data computed for κ and κ_u from both the VEOS and the parabolic fittings, respectively, with those obtained using the polyhedral contributions. The intervening relations are $\kappa=\frac{1}{2}(\kappa_{oct}+\kappa_{oct}^o)$ and $\kappa_u=\frac{1}{2}(\kappa_{oct}-\kappa_{oct}^o)$, and can be straightforwardly derived from $V=a^2c$ and Eqs. (4).

TABLE I. Zero-pressure structural data for anatase TiO_2. Lengths in Å and angles in degrees.

	Experimental	Calculated		
	Howard *et al.*[a]	This work (AE-B3LYP)	Fahmi *et al.*[b] (PS-HF)	Asahi *et al.*[c](AE-LDA)
a	3.785	3.7723	3.763	3.692
c	9.514	9.9285	9.851	9.471
c/a	2.513	2.632	2.618	2.566
u	0.208	0.2028	0.202	0.206
$d_{Ti\text{-}O}^{ap}$	1.978	2.013	1.995	1.948
$d_{Ti\text{-}O}^{eq}$	1.934	1.943	1.939	1.893
$d_{O\text{-}O}^{eq}$	2.793	2.827	2.824	2.740
$d_{O\text{-}O}^{sh}$	2.465	2.438	2.417	2.400
$d_{O\text{-}O}^{ush}$	3.040	3.117	3.099	3.002
2θ	156.16	152.09	157.56	152.1

[a]Reference 31.
[b]Reference 16.
[c]Reference 5.

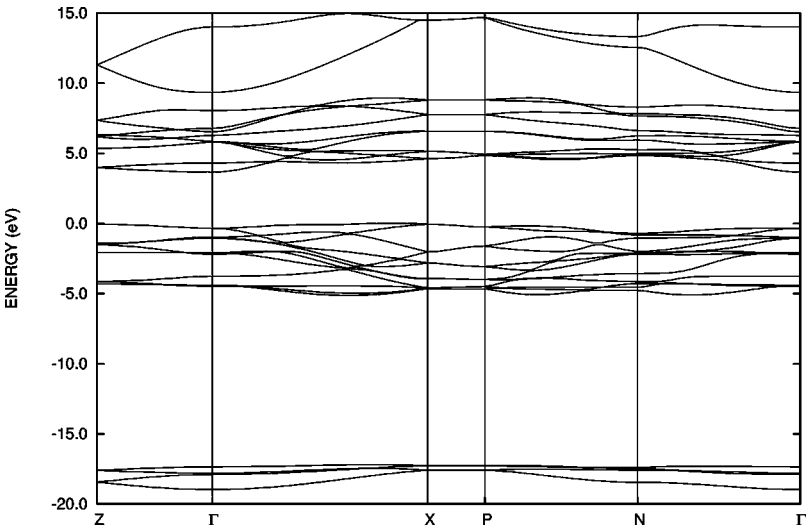

FIG. 3. Calculated band structure of anatase at the optimized equilibrium unit cell configuration.

III. RESULTS AND DISCUSSION

A. Unit cell geometry

A good description of the static equilibrium geometry is a requirement to validate the interpretation of volume-related bulk properties in terms of local magnitudes. Table I includes the structural parameters (a, c, u, θ, $d^{\mathrm{ap}}_{\mathrm{Ti\text{-}O}}$, $d^{\mathrm{eq}}_{\mathrm{Ti\text{-}O}}$, $d^{\mathrm{eq}}_{\mathrm{O\text{-}O}}$, $d^{\mathrm{sh}}_{\mathrm{O\text{-}O}}$, and $d^{\mathrm{ush}}_{\mathrm{O\text{-}O}}$) that describe anatase unit cell. Comparison with updated experimental data reveals that our computations are accurate enough, with deviations from the observed values never larger than 5%. Our calculated parameters agree also with the recent AE and PS results collected in the table.

B. Band structure and density of states

The computed band structure and the projected density of states at the equilibrium volume are presented in Figs. 3 and 4, where energies are referred to the Fermi level. Overall, the band structure features are in agreement with previous theoretical studies,[5,7,12,16] even though some of them consider crystallographic directions only adequate for tetragonal primitive structures. Comparison with the scarce experimental studies[18,28] dealing with the electronic structure of anatase is satisfactory. Sanjinés *et al.*[18] used photoemission spectromicroscopy to provide the main features of the core and valence bands, and to describe the experimental density of states of anatase. On the other hand, the oxygen $1s$ x-ray absorption spectra of de Groot *et al.*[28] determined the unoccupied states (up to 25 eV above the Fermi level) and were complemented with calculations using the localized spherical wave method.

The valence band (VB) is clearly divided into two sets of levels. The lowest one is centered at -17 eV and is composed of 4 bands that are associated with O $2s$ functions in a Mulliken decomposition. The second one, centered at -3 eV, is made up of 12 bands mainly corresponding to O $2p$ functions with a non-negligible contribution from Ti $3d$ functions. The upper VB possesses a bandwidth (VBW) of 5.05 eV, to be compared with theoretical values of 5.17 and 5.05 (see Refs. 12 and 5, respectively) and with the full width at half maximum experimental value of 4.70 ± 0.05 eV reported by Sanjinés *et al.*[18] The conduction band (CB) shows two regions: the one below 10 eV exhibits

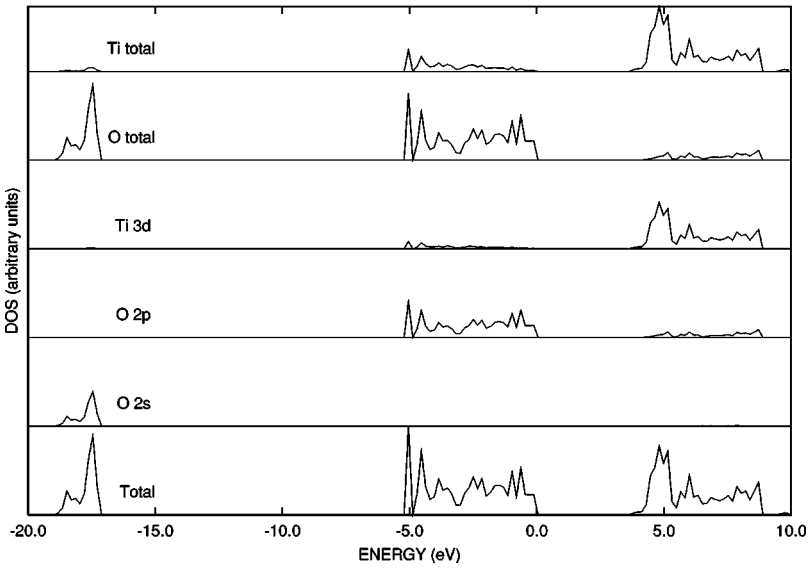

FIG. 4. Projected valence DOS of anatase from the band structure obtained at the optimized equilibrium unit cell configuration.

mainly Ti $3d$ character, and the one above 10 eV comes from Ti $4s$ and $4p$ orbitals. This is also in agreement with the analysis of de Groot *et al.*[28] The splitting between these two sets of bands is 1.31 eV at the optimized geometry. In general and as Mikami *et al.* have pointed out,[7] the planarity of these bands reflects the ionic character of this compound.

A closer look at the Mulliken partitions in the upper VB and lower CB has been traditionally used to obtain information about the chemical bonding. Due to the contribution of both Ti and O atoms to the VB and CB, a partial covalent character of the Ti-O bond is also suggested. Analogously to the detailed DOS analysis of Asahi *et al.*,[5] we find that the most important Ti-O mixing is σ and that it occurs at the bottom of the upper VB. The π mixture is much smaller, becoming negligible at the top of the VB, that is, almost exclusively composed of nonbonding O $2p$ functions. The lower CB (the one mainly associated with the Ti $3d$ orbitals) exhibits a very slight antibonding O $2p$ character, and displays two differentiated peaks coming from the t_{2g}-like, e_g-like crystal field splitting: a narrow segment below 6 eV and a wider one centered at about 8 eV. Along all this CB there is also a slight $2p$ oxygen character. We would like to point out that extracting chemical information from population analysis should be performed with care, particularly when small basis sets are employed. Cation-anion mixing may reflect in this case not an actual need, a covalent contribution, but just a way to improve the variational flexibility of the small set of atomic basis functions with those of the nearest neighbors.

We have obtained a minimal indirect band gap of 3.68 eV, less than 0.5 eV above the experimental value of 3.2 eV.[17] The bottom of the conduction band is found to be at Γ and the top of the valence band near X [at the point (0.0, 0.0, 0.44) in the BZ]. Previous studies[5,7,12,16] render a direct band gap of 2.0 eV and indirect band gap values ranging from 2.04 to 10.0 eV. According to our calculations, the direct band gaps at the Γ and X points are 4.02 and 4.37 eV, respectively, more than 0.3 eV above the indirect one at the predicted equilibrium geometry.

We have checked the stability of the above results against the crystal deformation induced by hydrostatic pressure. The description of the DOS is not qualitatively affected up to 15 GPa, where the unit cell volume is 7% lower than that at 0 GPa. The band gap remains indirect with a computed value of 3.78 eV at 14.83 GPa. At this pressure, the direct gap at Γ and the VBW increase to 4.21 eV and 5.24 eV, respectively. It is worthwhile to remark that, as pressure is applied, the bottom of the conduction band approaches the X point, (0,0,0.48) being its position at 14.83 GPa.

C. Bader analysis of the electronic density

Rigorous information about chemical bonding can be directly extracted from the topological analysis of the electron density. A first flavor is gained from consideration of the whole set of CP's of the crystalline electron density. This determines the chemical graph of the system. In our case and at the zero-pressure equilibrium geometry, three types of nonequivalent bonds appear in the unit cell. Two of them are the expected Ti-O links joining the cations to the apical and equatorial oxygens of a TiO_6 octahedron, respectively. We have also found one type of anion-anion bond between the nearest pairs of oxides, those that form the shared octahedral edges. All the other oxygen couples associated with the longer $d^{eq}_{O\text{-}O}$ and $d^{ush}_{O\text{-}O}$ distances do not share interatomic surfaces. In our empty oxygen tetrahedra, therefore, only one out of the six edges is an anion-anion link. Four ring CP's, one of them at the center of the empty octahedra, and only one type of minimum of the electron density inside a cage of bonds complete a consistent set of 96 CP's in the unit cell that fulfill the Morse's rule.[20]

The topological properties of bCP's are basic ingredients to understand the type of interaction between two atoms. It is found that Ti-O bonds display density values rather higher than those typical of clear closed-shell bonds. However, the Laplacian of the density, a measure of the local accumulation ($\nabla^2\rho<0$) or depletion ($\nabla^2\rho>0$) of the charge density in the bonding region, is positive. There is no shared electronic shell among the titanium and the oxygens, and the cation has lost its last atomic shell. Both kinds of Ti-O bonds are similar, but those involving the equatorial oxygens exhibit both slightly higher densities ($0.098e/\text{bohr}^3$ vs $0.085e/\text{bohr}^3$) and Laplacians ($0.518e/\text{bohr}^5$ vs $0.426e/\text{bohr}^5$) than the ones involving the apical oxygens. This fact is just a consequence of the logarithmic dependence of densities and their derivatives with interatomic distances. Summarizing, we have very polar Ti-O bonds that involve the interaction between small and quite charged cations and very polarized anions. On the other hand, O-O bonding turns out to be a typical closed-shell long-distance interaction exhibiting low density and low positive Laplacian values ($\rho=0.039e/\text{bohr}^3$, $\nabla^2\rho=0.138e/\text{bohr}^5$) at the bCP.

These features firmly place anatase at an intermediate position as the chemical bonding is regarded. Charged Ti and O atoms interact through intense electrostatic forces that highly distort the anionic charge distribution. Such an image is also found in other oxides like ZrO_2 or ZnO, for instance. Accordingly, our calculated atomic properties separate from those of purely ionic systems. The shape of the atoms in the crystal is found to be basically polyhedral. Ti is a rather compact distorted cube, whereas O is much bigger and irregular in order to completely fill the large free space left by the cations, around 80% of the unit cell volume. The topological charges computed by integrating the electron density within these basins, $\mathcal{Q}_{Ti}=2.96e$ and $\mathcal{Q}_O=-1.48e$, are smaller than those of nominal oxidation states, and the oxide's charge is clearly below the topological values obtained in prototype ionic oxides like MgO. As occurs with the band structure and the DOS, hydrostatic pressure does not modify the above picture. The electron density and Laplacian values at bCP's increase slightly, driven by bond length variations, but all the previously commented characteristics of the interactions survive compression. As a quantitative example, the AIM charge of Ti decreases by less than 1% on going from 0 to 15 GPa, the largest pressure here examined.

D. Analysis of pressure effects on the crystal geometry

Our computed values for the zero-pressure bulk modulus (B_0) and linear compressibilities (κ_a, κ_c) are compared with

TABLE II. Zero-pressure bulk modulus (GPa) and linear and bond length compressibilities (MPa^{-1}) (see text for definitions).

	Experimental	Calculated		
	Arlt *et al.* [a]	This work	Mikami *et al.* [b]	Arlt *et al.* [a]
B_0	179(2)-190(2)	200.34	187-196	189.5
B_0'	4.5(10)-5.3(10)	2.538		3.42
κ_a	1.00(2)	0.939		1.62
κ_c	3.30(2)	2.983		1.85
$\kappa(d^{ap}_{Ti\text{-}O})$		1.138		
$\kappa(d^{eq}_{Ti\text{-}O})$		1.520		
$\kappa(d^{eq}_{O\text{-}O})$		2.036		
$\kappa(d^{sh}_{O\text{-}O})$		-0.172		
$\kappa(d^{ush}_{O\text{-}O})$		2.235		

[a]Reference 6.
[b]Reference 7.

experiment and other theoretical results in Table II. The zero-pressure atomic and polyhedral volumes, fractional volume occupancies (f_i), and compressibilities are given in Table III. We have displayed the pressure evolution of the topological (V_{Ti}, V_O) and polyhedral (V_{oct}, V^o_{oct}, V^o_{tet}) volumes in Fig. 5, the lattice parameters (a, c) and the Ti-O and O-O distances in Fig. 6, and the internal parameter u and the c/a ratio in Fig. 7. Our computed B_0 is $\sim 5-12$ GPa greater than the experiment,[6] the *ab initio* perturbed ion result,[6] and the theoretical value reported by Mikami *et al.*[7] Linear compressibilities κ_a and κ_c agree fairly well with the experimental values. The compressibility along the c axis is 3 times larger than that corresponding to the a axis ($\kappa_c \simeq 3\kappa_a$), which is clearly a consequence of the alignment of the empty O_6 octahedra along the c axis and of the greater density of atoms along the a and b axes than along the c axis.

In the ideal $u=\frac{1}{4}$ structure, the unit cell volume is equally shared by the occupied octahedra, the empty octahedra, and the empty tetrahedra [see Eqs. (4)]. As u decreases from $\frac{1}{4}$, the splitting between f^o_{oct} and f_{oct} increases, whereas f^o_{tet} remains equal to $\frac{1}{3}$. In the present calculation $u=0.2028$, yielding significant deviations from the ideal values for f_{oct} and f^o_{oct}. The ratio f_{oct}/f^o_{oct} predicted by our calculations is 0.68, i.e., considerably smaller than 1.0. This behavior can be easily rationalized in terms of the oxygen competition between the occupied and empty octahedra. Occupied octahedra, with a central Ti atom, are much smaller than the empty ones, where the strongly attractive Ti-O interactions are absent. It is easily seen from Eqs. (4) that the condition for V_{oct} being smaller than V^o_{oct} is just $u<\frac{1}{4}$. Small, highly charged cations would favor low u values, while large cations would make the structure tend to the ideal case.

TABLE III. Decomposition of the bulk compressibility into local (atomic and polyhedral) contributions. Volumes in $Å^3$ and κ_0 in MPa^{-1}. o-oct, e-oct, and e-tet stand for occupied TiO_6 octahedra, empty O_6 octahedra, and empty O_4 tetrahedra, respectively.

	V_0	f_i	κ_0
bulk	35.34	1.000	4.992
o-oct	9.55	0.270	3.026
e-oct	14.00	0.396	6.097
e-tet	2.94	0.333	4.870
Ti	6.62	0.187	2.961
O	14.35	0.813	5.204

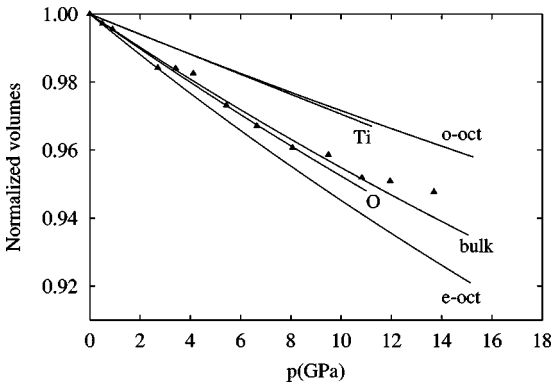

FIG. 5. Effect of hydrostatic pressure on crystal, polyhedral, and atomic normalized volumes according to our calculations (lines) and available experimental data (symbols). o-oct and e-oct stand for occupied octahedra and empty octahedra, respectively.

The existence of a Ti atom inside the occupied octahedron makes this polyhedron much more difficult to compress than the empty one: A decrease of the rather short Ti-O distances involves very repulsive core-valence Ti-O interactions. This effect is absent in the case of the empty O_6 octahedron. The final result is that κ^o_{oct} is almost twice the value of κ_{oct}. Since the magnitude of the splitting $\kappa^o_{oct}-\kappa_{oct}$ is determined by the pressure derivative of u (remember $2\kappa_u=\kappa_{oct}-\kappa^o_{oct}$), the above discussion suggests that u should increase with p. This is in fact the behavior observed in Fig. 7.

The increase (decrease) of u (c/a) with p can also be rationalized on the basis of the natural tendency of atoms to attain a closer packing upon crystal compression. This principle favors the regularity of the different polyhedra or, in terms of our geometrical parameters, the approach of u and c/a to $\frac{1}{4}$ and 2.0, respectively. As our zero-pressure values for these two magnitudes are $u<\frac{1}{4}$ and $c/a>2.0$, u and c/a must increase and decrease with p, respectively. The search

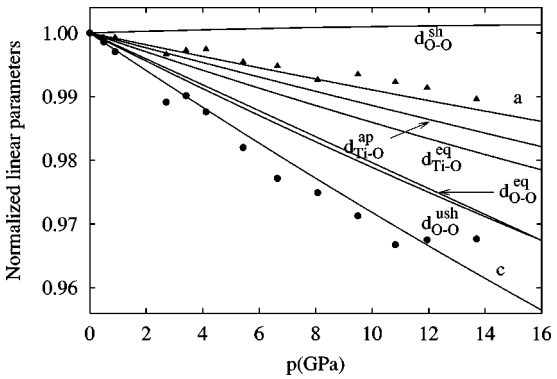

FIG. 6. Effects of hydrostatic pressure on the unit cell parameters and bond lengths according to our calculations (lines) and available experimental data (symbols).

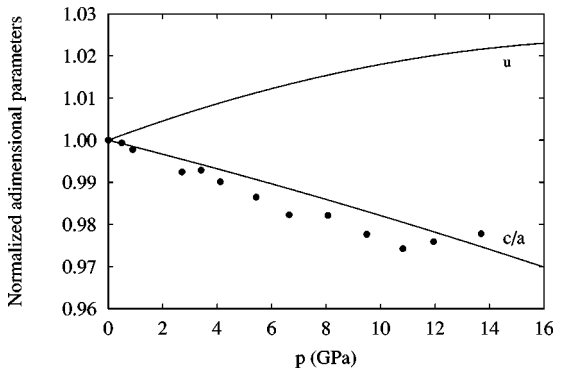

FIG. 7. Effects of hydrostatic pressure on the internal parameter u and c/a ratio according to our calculations (lines) and available experimental data (symbols).

for a closer atomic packing is also manifested in the progressive increase of the angle 2θ with p: We obtain $2\theta=152.1°$ at $p=0$, whereas the predicted value at 14.83 GPa is $2\theta=155.6°$.

We observe in Table III that more than 80% of the total cell volume is occupied by the AIM basins of the oxides. As a consequence the bulk compressibility, $\kappa=4.992\ \mathrm{MPa}^{-1}$, in agreement with what we have previously observed in a set of four related oxide spinels,[13] is mainly determined by the oxide's compressibility $\kappa_O=5.449\ \mathrm{MPa}^{-1}$. This explains why the relative magnitudes of V_O and V with respect to their zero-pressure values (normalized magnitudes in the following) run parallel as p increases (Fig. 5). One can also see in this figure that the normalized V_{Ti} and V_{oct} are practically coincident up to $p=10$ GPa. Figures. 5–7 show that our normalized V, a, c, and c/a vs p curves reproduce fairly well the available experimental data, despite the sometimes large dispersion of the latter. It is very interesting to compare the polyhedral and atomic compressibilities. For instance, the compressibility of the empty octahedra, the most compressible polyhedral entities of the structure, is only a rough 20% greater than that of the oxide basin. In the same spirit, the empty tetrahedra are best understood as space filled with oxide density. It is also to be noticed that despite a 30% of the volume of the occupied octahedra being with density coming from the anions, its compressibility is practically that of the bare Ti.

The pressure evolution of the Ti-O and O-O distances (d_i) can be analyzed in terms of the magnitudes

$$\kappa(d_i)=-\frac{1}{d_i}\left(\frac{\partial d_i}{\partial p}\right),$$

which can be obtained from the zero-pressure values of a, c, u, and κ_η ($\eta=a,c,u$) by differentiating Eqs. (1) and (2) with respect to p. The computed values of $\kappa(d_i)$ are collected in Table II. Their relative values are in complete agreement with the corresponding slopes of curves depicting the variation of the normalized linear parameters versus p (see Fig. 6). The increase of u with p tends to put the four equatorial O atoms of the TiO_6 octahedron in the same plane as the Ti atom. This effect stretches $d^{sh}_{O\text{-}O}$ and shortens $d^{ush}_{O\text{-}O}$. The decrease of a and c produces a shortening of all d_i distances. Both combined effects yield a significant decrease of $d^{ush}_{O\text{-}O}$ with p and have a negligible effect on $d^{sh}_{O\text{-}O}$. On the other hand, $\kappa(d^{ap}_{Ti\text{-}O})$ is given by $\kappa_c+\kappa_u$. The computed κ_c and κ_u values are $2.983\ \mathrm{MPa}^{-1}$ and $-1.845\ \mathrm{MPa}^{-1}$, respectively. The net effect is then a noticeable shortening of $d^{ap}_{Ti\text{-}O}$ as p increases. Finally, the Ti-O equatorial distance also shows a considerable decrease with p that can be explained using the analytical expression of $\kappa(d^{eq}_{Ti\text{-}O})$ derived from Eq. (1):

$$\kappa(d^{eq}_{Ti\text{-}O})=\frac{\frac{1}{4}a^2c\kappa_a+c^2\left(u-\frac{1}{4}\right)^2(\kappa_a+\kappa'_u)}{(d^{eq}_{Ti\text{-}O})^2},$$

$$\kappa'_u=\frac{1}{\frac{1}{4}-u}\left[\frac{d\left(u-\frac{1}{4}\right)}{dp}\right]. \tag{6}$$

All the magnitudes involved in Eqs. (6) are positive, being $\kappa'_u=7.923\ \mathrm{MPa}^{-1}$ at zero pressure.

IV. CONCLUSIONS

We have used a standard quantum-mechanical methodology based on the density functional approximation to investigate the structural, chemical bonding, and electronic behavior of the anatase phase of TiO_2 at static and high-pressure conditions. In addition, the AIM topological analysis of the electron density together with the decomposition of the unit cell volume into atomic and polyhedral regions has also been applied to complement and extend our study. Comparison with available experimental data and recent theoretical calculations shows that our computational strategy provides results that are accurate enough to contribute in a reliable manner to the understanding of the fundamental properties of anatase.

The exploration of the crystalline wave function shows that this compound exhibits both ionic and covalent features: flat bands but some Ti-O mixing at the valence and conduction bands; high values of the electron density at the bond critical points but positive Laplacian values. The actual charge for Ti is computed to be $3+$ according to the Bader analysis, not too far from the completely ionic value of $4+$. The bonding net consists of two different Ti-O bonds plus one O-O bond located in the TiO_6 shared edges. Pressures as high as 15 GPa (TiO_2 is not found in the anatase form above 13 GPa; see Ref. 6) do not modify qualitatively these results. The same occurs to the band structure. The band gap remains indirect ($\Gamma\rightarrow\sim X$) in all the pressure range studied, and increments of only 0.1 eV and 0.2 eV are found for the absorption edge and the VBW, respectively, on going from 0 to 15 GPa.

The macroscopic compression of anatase is mainly achieved through the deformation of the anions, whereas Ti

atoms behave as compact entities that only occupy 20% of the unit cell volume. This result allows us to explain the similarity of the bulk moduli (around 200 GPa) of oxide compounds with anionic close packing. As pressure is applied, the three elementary polyhedra of this structure reduce their volume at different rates. The TiO_6 octahedra are the most difficult to compress due to the Ti-O bonds. The contrary occurs to the O_6 octahedra, as they are empty and turn out to be bigger than the O_4 tetrahedra. The latter follow exactly the bulk behavior. As a result, the sign of the slope of the u vs p curve can be predicted, and it is found in agreement with our computations. These trends are interesting since, when transferred appropriately, they can be used to infer the response of more complex materials to hydrostatic pressure.

ACKNOWLEDGMENTS

We are grateful to the Spanish DGICYT, Project No. BQU2000-0466, for financial support. P.M.S. and J.M.R. thank the Spanish MECD for graduate and visiting professor grants, respectively. M.C. is grateful to the Conselleria de Cultura, Educacio i Ciencia (Generalitat Valenciana) for support. Use of the computer facilities of the Servei d'Informatica (Universitat Jaume I) is also acknowledged.

[1] A. Fujishima and K. Honda, Nature (London) **238**, 37 (1972).
[2] D.V. Ollis, E. Pelizzetti, and N. Serpone, in *Photocatalysis, Fundamentals and Applications*, edited by N. Serpone and E. Pelizzetti (Wiley, New York, 1989), p. 603.
[3] M. Grätzel, Comments Inorg. Chem. **31**, 567 (1992).
[4] H. Tang, K. Prasad, R. Sanjinés, P.E. Schmid, and F. Lévy, J. Appl. Phys. **75**, 2042 (1994).
[5] R. Asahi, Y. Taga, W. Mannstadt, and A.J. Freeman, Phys. Rev. B **61**, 7459 (2000).
[6] T. Arlt, M. Bermejo, M.A. Blanco, L. Gerward, J.Z. Jiang, J. Staun Olsen, and J.M. Recio, Phys. Rev. B **61**, 14 414 (2000).
[7] M. Mikami, S. Nakamura, O. Kitao, H. Arakawa, and X. Gonze, Jpn. J. Appl. Phys. **39**, L847 (2000).
[8] V. Swamy and J.D. Gale, Phys. Rev. B **62**, 5406 (2000).
[9] J. Haines and J.M. Léger, Physica B **192**, 233 (1993).
[10] K. Lagarec and S. Desgreniers, Solid State Commun. **94**, 519 (1995).
[11] J.K. Dewhurst and J.E. Lowther, Phys. Rev. B **54**, R3673 (1996).
[12] S-D. Mo and W.Y. Ching, Phys. Rev. B **51**, 13 023 (1995).
[13] A. Martín Pendás, A. Costales, M.A. Blanco, J.M. Recio, and V. Luaña, Phys. Rev. B **62**, 13 970 (2000).
[14] J.M. Recio, R. Franco, A. Martín Pendás, M.A. Blanco, and L. Pueyo, Phys. Rev. B **63**, 184101 (2001).
[15] P. Mori-Sánchez, R. Franco, A. Martín Pendás, V. Luaña, and J.M. Recio, Europhys. Lett. **54**, 760 (2001).
[16] A. Fahmi, C. Minot, B. Silvi, and M. Causá, Phys. Rev. B **47**, 11 717 (1993).
[17] H. Tang, H. Berger, P.E. Schmid, F. Lévy, and G. Burri, Solid State Commun. **23**, 161 (1977).
[18] R. Sanjinés, H. Tang, H. Berger, F. Gozzo, G. Margaritondo, and F. Lévy, J. Appl. Phys. **75**, 2945 (1994).
[19] R.F.W. Bader, *Atoms in Molecules* (Oxford University Press, Oxford, 1990).
[20] A. Martín Pendás, A. Costales, and V. Luaña, J. Phys. Chem. B **102**, 6937 (1998).
[21] V.R. Saunders, R. Dovesi, C. Roetti, M. Causá, N.M. Harrison, R. Orlando, and C.M. Zicovich-Wilson, *CRYSTAL98 User's Manual* (University of Torino, Torino, 1998).
[22] V.A. Rassolov, J.A. Pople, M.A. Ratner, and T.L. Windus, J. Chem. Phys. **109**, 1223 (1998).
[23] A.D. Becke, J. Chem. Phys. **98**, 5648 (1993).
[24] C. Lee, R.G. Yang, and R.G. Parr, Phys. Rev. B **37**, 785 (1988).
[25] C-H. Hu and D.P. Chong, in *Encyclopedia of Computational Chemistry*, edited by P. von Ragué Schleyer (Wiley, Chichester, 1998).
[26] C.J. Bradley and A.P. Crácknell, *The Mathematical Theory of Symmetry in Solids* (Clarendon Press, Oxford, 1972).
[27] J.A. Melder and R. Mead, Comput. J. (UK) **7**, 308 (1965).
[28] F.M.F. de Groot, J. Faber, J.J.M. Michiels, M.T. Czyzyk, M. Abbate, and J.C. Fuggle, Phys. Rev. B **48**, 2074 (1993).
[29] A. Martín Pendás and V. Luaña, *The Critic Program* (University of Oviedo, Oviedo, 1995).
[30] P. Vinet, J.H. Rose, J. Ferrante, and J.R. Smith, J. Phys.: Condens. Matter **1**, 1941 (1989).
[31] C.J. Howard, T.M. Sabine, and F. Dickson, Acta Crystallogr., Sect. B: Struct. Sci. **47**, 462 (1991).